UC San Diego
UC San Diego Previously Published Works

Title

In situ x-ray absorption investigations of a heterogenized molecular catalyst and its interaction with a carbon nanotube support

Permalink

Journal

ISSN

Authors

Zoric, Marija R
Chan, Thomas
Musgrave, Charles B
et al.

Publication Date

DOI

In situ x-ray absorption investigations of a heterogenized molecular catalyst and its interaction with a carbon nanotube support

Marija R. Zoric ; Thomas Chan ; Charles B. Musgrave, III ; William A. Goddard, III ; Clifford P. Kubiak; Amy A. Cordones

Check for updates

View Online

Export Citation

CrossMark

18 July 2023 16:41:10

In situ x-ray absorption investigations of a heterogenized molecular catalyst and its interaction with a carbon nanotube support

View Online   Export Citation   CrossMark

Marija R. Zoric,[1] [iD] Thomas Chan,[2] [iD] Charles B. Musgrave III,[3] [iD] William A. Goddard III,[3] [iD] Clifford P. Kubiak,[2] and Amy A. Cordones[1,a) [iD]

AFFILIATIONS

[1] Stanford SUNCAT Institute, Stanford PULSE Institute, SLAC National Accelerator Laboratory, Menlo Park, California 94025, USA
[2] Department of Chemistry and Biochemistry, University of California at San Diego, La Jolla, California 92093, USA
[3] Materials and Process Simulation Center, California Institute of Technology, Pasadena, California 91125, USA

Note: This paper is part of the JCP Special Topic on In situ and Operando Characterization.
[a)] Author to whom correspondence should be addressed: acordon@slac.stanford.edu

ABSTRACT

A highly active heterogenized molecular CO_2 reduction catalyst on a conductive carbon support is investigated to identify if its improved catalytic activity can be attributed to strong electronic interactions between catalyst and support. The molecular structure and electronic character of a $[Re^{+1}(tBu\text{-}bpy)(CO)_3Cl]$ (tBu-bpy = 4,4′-tert-butyl-2,2′-bipyridine) catalyst deposited on multiwalled carbon nanotubes are characterized using Re L_3-edge x-ray absorption spectroscopy under electrochemical conditions and compared to the homogeneous catalyst. The Re oxidation state is characterized from the near-edge absorption region, while structural changes of the catalyst are assessed from the extended x-ray absorption fine structure under reducing conditions. Chloride ligand dissociation and a Re-centered reduction are both observed under applied reducing potential. The results confirm weak coupling of $[Re(tBu\text{-}bpy)(CO)_3Cl]$ with the support, since the supported catalyst exhibits the same oxidation changes as the homogeneous case. However, these results do *not* preclude strong interactions between a *reduced* catalyst intermediate and the support, preliminarily investigated here using quantum mechanical calculations. Thus, our results suggest that complicated linkage schemes and strong electronic interactions with the initial catalyst species are not required to improve the activity of heterogenized molecular catalysts.

INTRODUCTION

Electrocatalytic reduction of carbon dioxide coupled with renewable energy, such as solar, can provide a promising way to form green fuels. Considering the plethora of possible reduction products, the catalyst must provide high product selectivity for this application. Molecular catalysts, having well-defined reaction centers, are generally more selective than their heterogeneous counterparts and present ideal platforms for elucidation of structure–activity relationships.[1,2] However, homogeneous catalysis in solution presents challenges in product separation and isolation while making use of only a small fraction of the electroactive catalyst, which is located necessarily in the diffusion-reaction layer of the electrode. To address these issues, there has been significant interest in heterogenizing molecular catalysts on conductive supports. Such heterogenized systems require low catalyst loading while maintaining the selectivity, tunability, and efficiency of the molecular catalyst.[1,3]

In heterogenized catalysts, the surface-immobilized species are electroactive; thus, large surface area supports, such as porous

18 July 2023 16:41:10

electrodes,[1,4] gas diffusion electrodes,[5] and carbon nanostructures,[6–9] have been explored. The catalyst is often supported by the electrode through π-π stacking interactions or covalent bonding, such that the catalyst preserves the electronic and structural properties of the homogeneous molecular system and therefore operates with the same catalytic mechanism. Alternatively, cases of molecular catalysts strongly coupled electronically to a conductive support have been demonstrated, in which the catalyst electronic states are no longer distinguishable from those of the electrode.[10–12] This is typically achieved by a covalent linkage,[11–13] or in rare cases by strong π-π stacking,[14] of the catalyst and support. Strong electronic coupling has important implications for catalysis since it can avoid the high energy redox intermediates involved in homogeneous catalysis; instead coupling electron transfer and substrate activation steps to increase catalytic activity.[10–12]

[Re^{+1}(tBu-bpy)(CO)$_3$Cl] [fac-Re(4,4′-tert-butyl-2,2′-bipyridine)-(CO)$_3$Cl, termed here as Re^{+1}-chloro and shown in Scheme 1(a)], is one of the most robust homogeneous molecular catalysts for CO$_2$ reduction (CO$_2$RR).[15,16] It was reported to convert CO$_2$-to-CO with high (>99%) faradaic efficiency (FE).[16] In addition, this family of Re-based catalysts have been non-covalently[17,18] and covalently attached to electrode surfaces[13,19,20] and imbedded into polymer films,[21] to form heterogenized catalysts. Notably, immobilization of the Re^{+1}-chloro catalyst on multiwalled carbon nanotubes (CNTs) led to improved catalytic behavior compared to the homogeneous system: including lower overpotential, higher FE, and constant CO production for longer operation times.[22] Furthermore, the heterogenized catalyst showed these improvements in aqueous medium (in contrast to the organic solvent electrolytes used for homogeneous catalysis) despite the lower solubility of CO$_2$ in water.[16,22] While a full explanation for the enhanced catalytic properties of the heterogenized system was not established, it was noted that sequential cyclic voltammograms (CVs) led to disappearance of faradaic features.[22] This is consistent with the absence of CV peaks previously demonstrated for strongly coupled catalyst/electrode systems.[10–13] This intriguing similarity leads to questions regarding the strength of catalyst–support interactions in this system that does not have the direct covalent linkage or large conjugated structures present in previous examples of strongly coupled systems,[10–14] but still exhibits enhanced catalysis.

In this work, the interactions between the Re^{+1}-chloro catalyst and conductive CNT support are investigated using Re L$_3$-edge x-ray absorption spectroscopy (XAS). The near-edge region (XANES, x-ray absorption near-edge structure) of transition metal complex L-edge spectra is characterized by large dipole-allowed transitions of 2p core electrons to unoccupied orbitals with metal d character (Re 5d, in this case). The Re L$_3$-edge XANES region is therefore sensitive to the Re oxidation state and is used here to probe metal reduction in Re^{+1}-chloro under applied potential. Re L$_3$-edge XANES has been used previously to investigate the electronic structure of Re(bpy)(CO)$_3$X (X = Cl, Br) complexes[23,24] and their homogeneously reduced analogs.[25] The in situ XANES approach applied here has also been used previously to distinguish the differences in oxidation state changes occurring in other weak or strong electronically coupled molecular catalyst/support systems.[11,12] Additionally, the extended x-ray absorption fine structure (EXAFS) region of the XAS spectrum is sensitive to metal–ligand bonding, which we use here to investigate structural
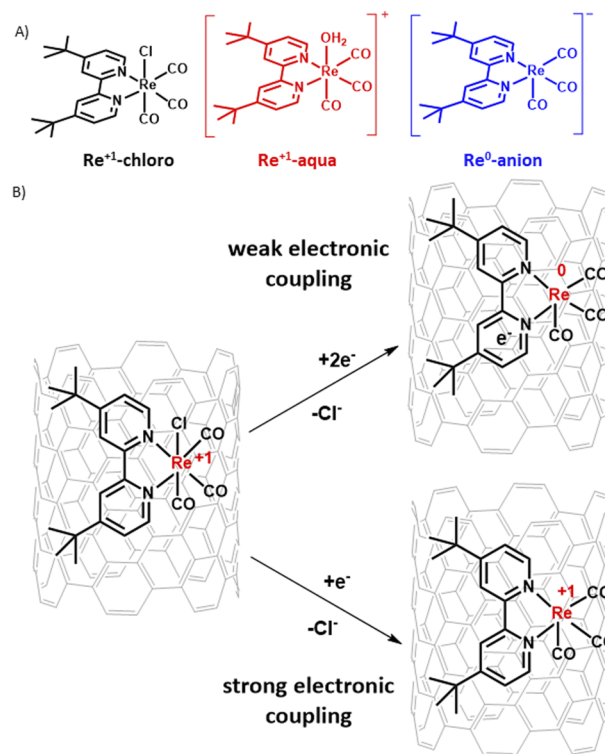
SCHEME 1. (a) Structures of the catalyst and reference compounds used in this study. Illustration of Re@CNT and expected behavior upon reduction in the case of weak (upper panel) and strong (lower panel) catalyst–CNT electronic coupling.

changes of the catalyst upon heterogenization, as well as under applied reducing bias. We demonstrate that the Re^{+1}-chloro catalyst does *not* have strong electronic communication with the CNT support.

RESULTS AND DISSCUSION

The heterogenized electrodes [Re@CNT, Scheme 1(b)] were prepared by spray coating a suspension of Re^{+1}-chloro catalyst and CNTs onto carbon fiber paper (used as a current collector). The same preparation of Re@CNT was previously demonstrated for CO$_2$RR catalysis, showing improved performance toward CO production compared to the homogeneous catalyst analog.[22] Here, the Re L$_3$-edge XAS was measured at the Stanford Synchrotron Radiation Lightsource beamline 9-3 under reducing conditions using an in situ electrochemical flow cell (Fig. S1) to identify the electronic and structural properties of the heterogenized Re@CNT catalyst. The CV of Re@CNT measured in the in situ x-ray cell (Fig. S2) matches that which was reported previously,[22] including the decreasing faradaic current upon successive scanning.

The response of the XAS spectrum to applied cathodic potential is expected to reflect the strength of catalyst–CNT electronic coupling, as described below and demonstrated previously.[11,12] Under homogeneous conditions (acetonitrile solvent), the Re^{+1}-chloro complex first undergoes a reversible one electron reduction that is

thought to be bpy-centered based on x-ray and IR spectroscopy.[25–27] This is followed by an irreversible second reduction, thought to be metal centered (Re^{+1} to Re^0), accompanied by Cl^- ligand dissociation.[20,25–27] On the basis of the above assignments of ligand- and metal-centered reductions, we refer to the two-electron reduced active catalyst species as $[Re^0(tBu-bpy^-)(CO)_3]^-$ [termed here Re^0-anion and shown in Scheme 1(a)]. For Re@CNT, if the molecule is not strongly coupled to the electrode states [Scheme 1(b), upper pathway], then it should behave essentially as the homogeneous molecule, accepting two electrons from the electrode to form the Re^0-anion species. However, if the molecule is strongly coupled to the electrode states, then varying the potential should not change the driving force for electron transfer.[10] In this case, electron transfer would occur only when compensating for ion transfer (Cl^- dissociation) to form $[Re^{+1}(tBu-bpy)(CO)_3]$ [Scheme 1(b), lower pathway].[10–12] This implies no change in the Re oxidation state if the catalyst is strongly coupled to the CNT support. In both the weak and strong coupling scenarios, dissociation of the Cl^- ligand is expected upon reduction and is monitored by Re L_3-edge EXAFS to ensure that a large electroactive fraction of catalyst is present. The difference in Re oxidation state for the two scenarios is probed by changes in the Re L_3-edge XANES strong absorption peak (often referred to as the white line absorption peak), which measures $2p_{3/2}$-to-5d transitions and is therefore sensitive to the Re 5d electron occupation.[23,25] The XANES white line feature is expected to decrease in intensity upon reduction in the weak coupling case (reflecting the change from +1 to 0 Re oxidation state),[25] while no spectral changes are expected in the strong coupling case, as was demonstrated before for strongly coupled Rh-based catalysts.[11,12]

The homogeneous catalyst reference complexes shown in Scheme 1(a) are used to directly predict changes in Re L_3-edge XANES and EXAFS upon Cl^- dissociation or upon metal reduction. $[Re^{+1}(tBu-bpy)(CO)_3(H_2O)]^+$ (termed Re^{+1}-aqua) has the same Re oxidation state as Re^{+1}-chloro, but the Cl^- ligand has been replaced by a labile water ligand. Re^0-anion is formed following the two-electron chemical reduction of the Re^{+1}-chloro complex and Cl-ligand dissociation.[25] The Re L_3-edge XAS spectra of the three reference complexes are shown in Fig. 1. The XANES region shown in panel A is comprised of a strong white line feature, enhanced in Re carbonyl complexes due to mixing of the Re 5d and unoccupied carbonyl π^* orbitals.[25] The XANES white line intensity does not change significantly between the two Re^{+1} species, consistent with a lack of X ligand dependence reported previously for a series $Re(bpy)(CO)_3X$ complexes.[23] The Re^0-anion species has lower white line intensity than either Re^{+1} reference species due to the decreased Re oxidation state, consistent with previous reports.[25] The change in oxidation state can be approximated from the integrated $L_{2,3}$-edge absorption intensity, which is proportional to the number of Re 5d holes.[28] While only the L_3-edge was measured here, previous studies have shown the integrated intensity of the L_3-edge white line also depends linearly on the oxidation state.[29,30] We observe a decrease in the L_3-edge white line area of 18.2% (see Fig. S3 for analysis details). Assuming proportionality with the number of electron holes of the $5d^6$ Re^{+1}-chloro complex, our results indicate a decrease in oxidation state by 0.7 electrons upon forming the two-electron reduced Re^0-anion species. This intensity difference also indicates the expected XANES changes for the Re@CNT system if
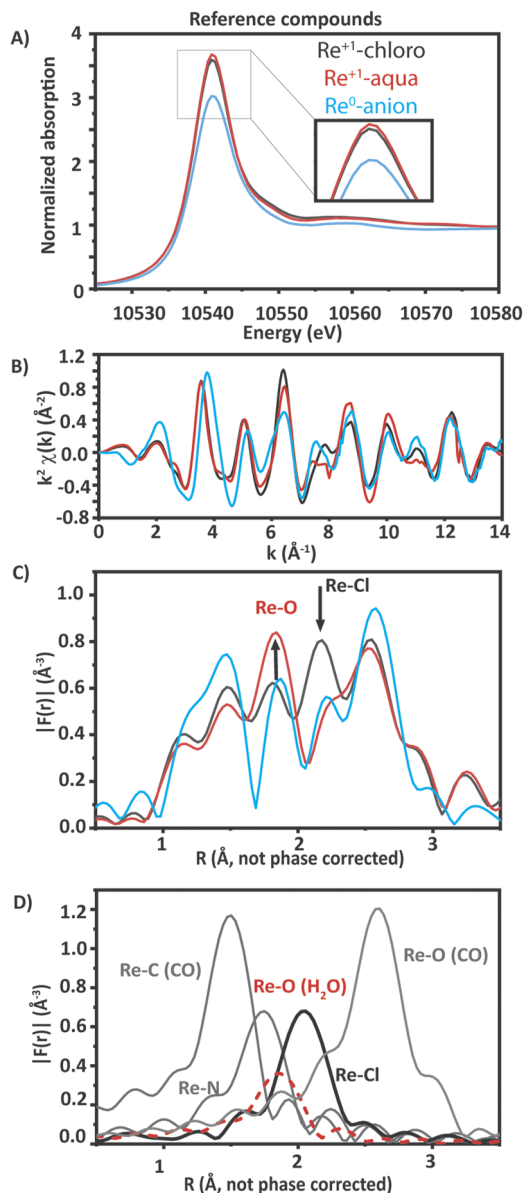

FIG. 1. Re L_3-edge XAS spectra for Re^{+1}-chloro (black), Re^{+1}-aqua (red), and Re^0-anion (blue) reference complexes: (a) XANES, (b) EXAFS in k space, and (c) Fourier transformed EXAFS in R space (k^2-weighted). (d) Calculated EXAFS peaks corresponding to the single scattering paths for Re^{+1}-chloro based on the crystal structure data[15] (solid lines), with the addition of the Re–O (H_2O) path (dashed red line) of Re^{+1}-aqua. Each trace shows the sum of single scattering paths for the specified Re-ligand bond type (i.e., the sum of three Re–C paths, two Re–N paths, etc.).

all of the Re^{+1}-chloro complex is reduced under applied potential, as would be expected for the weak electronic coupling scenario shown in Scheme 1(b).

The experimental EXAFS data for the three references is shown in Fig. 1(b) as a function of wavevector k and in panel C after

Fourier transform into R space (without phase correction). Calculated scattering paths for Re^{+1}-chloro and Re^{+1}-aqua (Re–O bond of aqua ligand only) are shown in panel D to aid in the assignment of EXAFS peaks to specific Re-ligand bond distances. Critical to this work is the Re–Cl bond distance observed at 2.2 Å (not phase corrected) for Re^{+1}-chloro. Upon Cl^--to-aqua ligand substitution, this peak decreases while a new Re–O (H_2O) peak appears at 1.8 Å (not phase corrected, overlapping with the Re–N (bpy) peak already present at similar distance). Similarly, Re^0-anion shows decreased intensity at the Re–Cl distance, as expected for the doubly reduced species. Regardless of the coupling strength, Cl^- ligand dissociation is expected under applied cathodic bias for Re@CNT, which will result in a decrease of this same EXAFS feature.

For the heterogenized Re@CNT catalyst, we evaluated if the molecular properties of Re^{+1}-chloro are changed by electrode preparation. Re^{+1}-chloro was mixed with CNTs as a suspension either in dry isopropyl alcohol (IPA) or in an IPA/water mixture (1:1 volume ratio) prior to spray coating on a carbon fiber paper current collector. The Re L_3-edge XAS was measured for the as-prepared electrodes ex situ as shown in Fig. 2. The EXAFS of Re^{+1}-chloro is unchanged in Re@CNT prepared from dry solvent, implying that
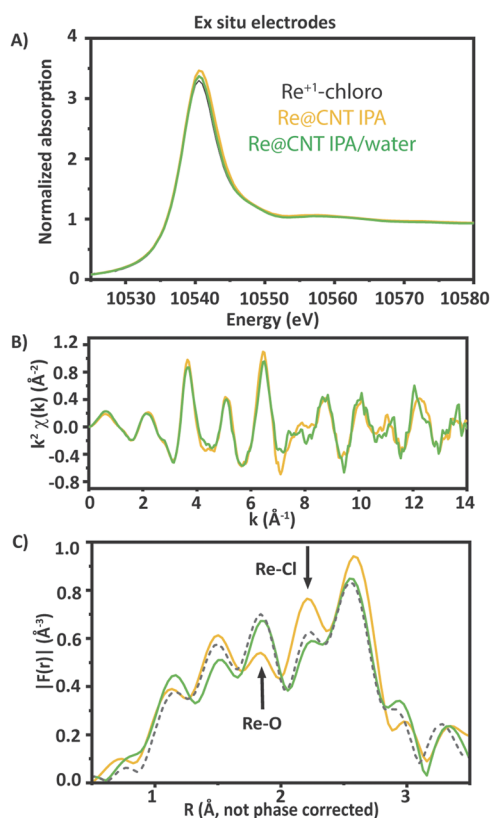

FIG. 2. Re L_3-edge XAS spectra for dry electrodes as-prepared from IPA (yellow) and IPA/water (green). (a) XANES spectra of the as-prepared electrodes and Re^{+1}-chloro (black) for comparison, (b) EXAFS spectra in k space, and (c) R space plotted with the linear combination fit (dashed gray line) of the Re@CNT IPA/water electrode (54% Re^{+1}-aqua, 46% Re^{+1}-chloro).

the molecular structure of Re^{+1}-chloro stays intact when deposited onto CNT. However, the introduction of water, either during the electrode preparation (green trace, Fig. 2) or through exposure to electrolyte in situ (Fig. 3), results in a decreased Re–Cl peak and increased Re–O peak, indicating that Cl^--to-water ligand exchange occurs in the aqueous environment. We find that 54% of the heterogenized catalyst is in the water-ligated form when Re@CNT is prepared from aqueous solvent using a linear combination fitting of the Re@CNT IPA/water XAS data with the Re^{+1}-chloro and Re^{+1}-aqua standards (Fig. S4). We find that ligand substitution continues to increase with in situ exposure to aqueous electrolyte, resulting in larger fractions of the water-ligated form (described below).

In situ XAS of the heterogenized Re@CNT catalyst was measured under argon in aqueous 0.5M $KHCO_3$ electrolyte to reproduce the catalytic conditions of Ref. 22. Figure 3 shows the XAS spectra of Re@CNT collected under open circuit potential (OCP) and then under applied negative bias sufficient to reduce the catalyst (−1.3 V vs Ag/AgCl applied as controlled potential electrolysis, CPE). As the loading conditions may influence the electroactive fraction of catalyst,[22,31,32] two loadings were explored: low Re loading (0.008 mg/cm^2, atomic ratio of CNT C atoms to catalyst Re atoms N_C/N_{Re} = 1800, Fig. 3) and high Re loading (0.06 mg/cm^2, N_C/N_{Re} = 332, Fig. S5). The Re–Cl EXAFS feature was monitored to confirm the electroactive catalyst fraction (defined as the fraction of pre-catalyst molecules that participate in the electrochemical reaction, regardless of coupling strength). This fraction can be quantified from the Re–Cl EXAFS feature in either strong or weak coupling scenarios, as both cases predict Cl^- ligand dissociation to form five-coordinate species. Under high loading conditions, no Cl^- dissociation is observed under applied potential (EXAFS unchanged), indicating that the electroactive fraction is too small to be observed by EXAFS (Fig. S5). Under low loading conditions, the Re–Cl peak in the EXAFS diminishes under applied potential [Fig. 3(c)], indicating the electroactive fraction is sufficient to be probed by XAS. This seemingly minor point demonstrates the importance of establishing the electroactive fraction independent of the in situ XANES measurement. Under high loading conditions, the lack of change in XANES could be interpreted as strong electronic coupling when in fact it should instead be attributed to a very small electroactive fraction.

The in situ XANES spectra of the low loading Re@CNT system is compared under OCP and CPE conditions to distinguish weak and strong electronic communication of the Re^{+1}-chloro catalyst with CNT support in Fig. 3(a). A decrease in the white line intensity (normalized to a constant edge jump) is observed upon reduction. This is consistent with the Re-centered reduction (from Re^{+1} to Re^0) indicative of weak electronic coupling, as illustrated in Scheme 1(b) (top panel). The magnitude of decrease in integrated white line intensity is, however, significantly smaller in the in situ measurements (−3.1%) compared to the Re^{+1} and Re^0 reference measurements (−18.2%). This can have two possible causes: (1) The catalyst is weakly coupled with the support, but only a small fraction is electroactive, or (2) some of the catalyst is strongly coupled with the carbon electrode (no change in XANES expected) while the rest is weakly coupled (change in XANES expected).

To distinguish these possibilities, we first performed a linear combination fitting of the EXAFS data (weighted by k^2, over range of 3–13.3 $Å^{-1}$) of the OCP and CPE in situ datasets using the
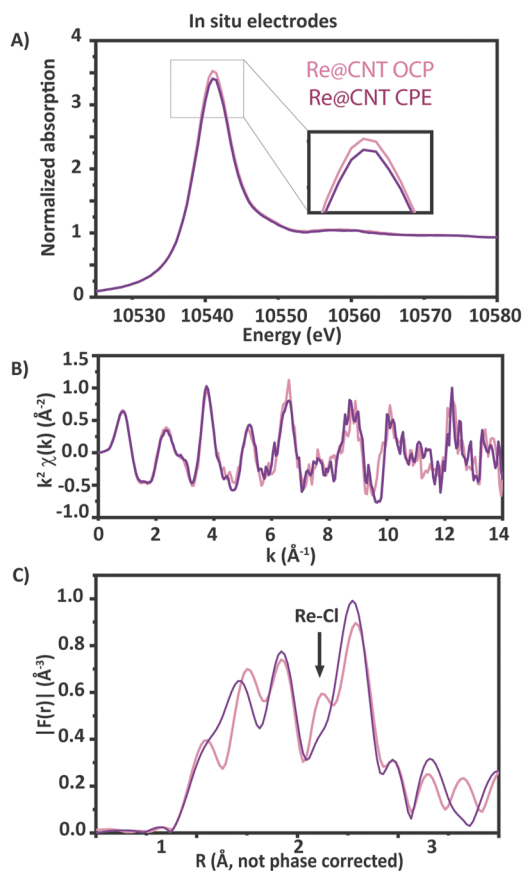
FIG. 3. Re L_3-edge spectra for Re@CNT under open circuit potential [pink, (a)–(c)] and reducing potential [purple, (a)–(c)]: (a) XANES spectra, (b) k space EXAFS spectra, and (c) R space k^2-weighted EXAFS spectra. The decrease in Re–Cl bonding indicated by the arrow in (c) indicates a significant electroactive fraction, while the decreased white line intensity in (a) indicates a change in Re oxidation state.

reference complex spectra. By fitting only the EXAFS region, the results determine the overall fraction of electroactive molecules based on changes in the Re coordination environment alone. This method is insensitive to the electronic coupling strength, as both strong or weak coupling will result in Cl$^-$ dissociation. We find that under OCP conditions, Re@CNT contains 31% Re^{+1}-chloro and 69% Re^{+1}-aqua species (Fig. S6). Under applied cathodic potential, we observe 14% more Cl-to-aqua ligand exchange (83% Re^{+1}-aqua, due to the longer water exposure time) and 17% electroactive fraction (17% of five-coordinate species formed, as modeled here by the Re^0-anion species EXAFS).

The results from the fits of the EXAFS data were then compared to the XANES region to assess if all of the electroactive species undergo a change in Re oxidation state under reducing bias, thus distinguishing the presence of a strongly vs weakly coupled system. If all of the electroactive fraction is weakly coupled, one expects the XANES white line integrated intensity to decrease by 3.1%. This prediction is derived from the decreased white line intensity of the reduced reference complex XANES spectrum (−18.2%), scaled

according to the electroactive fraction extracted from the EXAFS fit results (17%). If some fraction of the electroactive molecules are strongly coupled, the XANES white line peak will decrease by less than 3.1%, proportional to the strongly coupled fraction. Instead, from the *in situ* XANES, we find that the white line feature is observed to decrease by 3.1% upon reduction (see Fig. S7 for analysis details). This is in excellent agreement with the expectation for a weakly coupled system.

Our XAS analysis indicates weak electronic coupling between the Re^{+1}-chloro catalyst and CNT support, suggesting that the disappearance of the CV peaks observed upon consecutive scanning[22] cannot be explained by strong electronic communication with this catalyst species. It is perhaps not surprising that the six-coordinate Re^{+1}-chloro complex cannot support direct interactions between the metal center and CNT. However, we speculate that upon reduction it is possible that the five-coordinate reduced species, Re^0-anion, could support a stronger metal–CNT interaction. Such strong metal–CNT interactions were previously reported for reduced Re carbonyl complexes with open metal coordination sites {for example, Re^0(CO)$_5$ and [Re^{-1}(CO)$_4$]$^-$ species}, which are proposed to bond with fullerene supports based on IR spectroscopy and density functional theory calculations.[33,34] Based on the experiments reported here, a preliminary assessment of possible Re–CNT interactions is made on the comparison of the EXAFS measured *in situ* under cathodic potential to that calculated for a closely interacting system.

In order to make a comparison with these experimental results, we optimized the structure of an interacting Re^0-anion species and CNT fragment using density functional theory (DFT) [Fig. S8(a)]. In this structure, we found the distance between Re and the two closest CNT C atoms to be 2.86 Å with the corresponding Re–C scattering path centered at 2.42 Å without phase correction [Fig. S8(b)]. This DFT prediction is consistent with the increased EXAFS intensity observed at 2.48 Å under cathodic bias in Fig. 3(c) [whereas for the homogeneous reference complexes, the EXAFS intensity also increases but shifts to higher, not lower, R values compared to Re^{+1}-chloro, as shown in Fig. 1(c)]. At the short interaction distances predicted for the optimized structure, Re^0-anion may reside inside the electrical double layer. This could cause disappearance of the faradaic current because there would be no potential drop between the electrode and molecule to drive electron transfer, as shown previously.[35] While the EXAFS observations support the possibility of strong Re^0-anion/CNT interactions, further investigations are required to provide definitive evidence.

CONCLUSIONS

In conclusion, we demonstrate here that the Re^{+1}-chloro catalyst is weakly coupled to a CNT support in the heterogenized Re@CNT system using *in situ* Re L_3-edge XAS measurements. EXAFS was used to assess the coordination environment of the Re atoms, quantifying the electroactive fraction of catalyst (strong or weakly coupled) from the degree of Cl$^-$ ligand dissociation under reducing conditions. XANES was used to quantify the change in Re oxidation state in Re@CNT by comparison with the reduced catalyst reference complex. From comparing the EXAFS and XANES results, we observe that all of the electroactive catalyst undergoes

18 July 2023 16:41:10

Re-centered reduction, consistent with a weak electronic coupling scenario. Thus, strong Re^{+1}-chloro/CNT interactions cannot explain the diminished faradaic current observed in the heterogenized catalyst system. Instead, we hypothesize that the lack of CV features may be attributed to a short interaction distance between the five-coordinate reduced species Re^0-anion and CNT, which likely resides within the electrical double layer, as predicted by quantum mechanical (QM) calculations. This would suggest that improved catalytic behavior of Re^{+1}-chloro can be achieved by electrochemical treatment, instead of more synthetically complicated covalent linkage schemes, consistent with a previous observation for heterogenized Co phthalocyanine catalysts.[36]

EXPERIMENTAL SECTION

General methods

All reagents and solvents were purchased from commercial sources and used without further purification unless otherwise noted. IR was collected in N_2-filled glove box as a pellet in KBr (10% by mass). Electrochemical measurements were performed on a BioLogic SP-200 potentiostat. Proton nuclear magnetic resonance (NMR) was collected on Jeol NMR spectrometer operating at 400 MHz (^1H NMR).

Synthesis

Re^{+1}-chloro ([Re(tBu-bpy)(CO)$_3$Cl]): The previously published procedure was followed.[15] In brief, 323 mg (0.89 mmol) of Re(CO)$_5$Cl and 240 mg of 4,4′-di-tert-butyl-2,2′-dipyridyl (0.89 mmol) were heated to reflux in toluene overnight. The flask was then placed in the freezer to precipitate the product, which was vacuum filtered and rinsed with cold diethyl ether. The product was further purified by dissolving in a minimal amount of tetrahydrofuran (THF) and layering with excess hexanes in the freezer to yield 405 mg (79% yield). The product was characterized by FT-IR and ^1H NMR, which matched previously published data.[15]

Re^{+1}-aqua ([Re(tBu-bpy)(CO)$_3$(H$_2$O)](CF$_3$SO$_3$)). Re^{+1}-aqua was prepared using a modified published procedure.[37] 10 mg (0.017 mmol) of Re^{+1}-chloro was dissolved in 4 ml of dry acetone, followed by the addition of 5.2 mg (0.02 mmol) of silver triflate. The reaction mixture was stirred and heated to reflux in the dark for 4 h. The solution was filtered to remove AgCl formed during reaction. The mixture was concentrated on a rotary evaporator, followed by the addition of 1.6 ml deionized water to form Re^{+1}-aqua as an off-white precipitate. The mixture was filtered to yield 7.3 mg (0.01 mmol, 60%) of Re^{+1}-aqua complex.

Re^0-anion ([Re(tBu-bpy)(CO)$_3$] [K(18-crown-6)]). 29 mg (0.08 mmol) of Re^{+1}-chloro and 79 mg (0.3 mmol) of 18-crown-6 in 17 ml of THF was placed in the freezer at $-20\,^{\circ}$C. 41 mg (0.3 mmol) of KC$_8$ was added slowly to the stirring solution. The reaction is completed once the solution was heated up to room temperature, indicated by formation of a dark green color product. The total solution with filtered over celite. The product was further purified by dissolving in a minimal amount of THF and layering with excess pentane at room temperature. The solution was decanted off and the bottom product was vacuum dried. The crystallized product was dark red and characterized by FT-IR, in good agreement with previously published data.[15]

Electrodes preparation

Multiwalled carbon nanotube (MWCNT) preparation: The MWCNTs were purchased from Sigma-Aldrich (product 724769, 6–9 nm OD, 5 μm length) and then purified with 1M trace metal hydrochloric acid. The MWCNTs was added to the HCl solution to make a 1 mg/ml solution, followed by sonication for 1 h. The solution was then stirred for 22 h on a stir plate followed by another hour of sonication. The MWCNTs were vacuum filtered and then rinsed with MiliQ deionized water until the water rinsed off was pH neutral (checked with pH strips). The MWCNTs were dried under vacuum and heated on a rotary evaporator. As-prepared MWCNTs were characterized with Raman and IR spectroscopy to determine the quality of MWCNTs.

Preparation of Re^{+1}-chloro/MWCNT/CFP electrodes (Re@CNT): The selected amount of Re^{+1}-chloro catalyst (0.07 mg for thick electrodes and 0.013 mg for thin electrodes) and 5 mg of MWCNT are added to the IPA/water mixture (1:1 volume ratio) or dry IPA for dry electrodes. The solution was sonicated for 1 h. The ink solution was added to the spray coater. Carbon fiber paper (AvCarb, MGL 190) was cut into 4 × 2 cm^2 strips, rinsed with IPA, and sonicated for 1 min to clean the surface. Teflon tape was wrapped around the sides to make a 2 × 2 cm^2 area for coating. The electrode was heated on a hot plate at 80 $^{\circ}$C while spray coating. Each layer was coated from a uniform distance between the spray coater and the sample upon drying of the previous layer. Following catalyst application, the electrode was dried at 80 $^{\circ}$C on the hot plate for 1 h. The mass before and after spray coating was taken to determine the catalyst/MWCNT loading on the electrode of 0.345 mg/cm^2 (regardless of catalyst/MWCNT ratio).

X-ray absorption spectroscopy

Re L$_3$-edge XAS was performed at Beamline 9-3 of the Stanford Synchrotron Radiation Lightsource (SSRL). All data were collected at room temperature. XAS measurements were made both using transmission geometry and by detecting the total fluorescence yield (TFY). Ion chamber detectors before and after the sample were used for transmission measurements. TFY measured at 90° with respect to the incident beam used either a PIPS diode (for reference complex measurements) or 100-channel germanium detector (for electrode measurements), positioned behind a Cu filter and Soller slit assembly to minimize elastic scatter. A Si(220) double crystal monochromator ($\varphi = 0^{\circ}$) was used to scan the incident x-ray energy. A portion of the incident beam was transmitted through a 12.5 μm thick Re foil, which was used as a calibration standard with the first inflection point set to 10 535.0 eV. The x-ray spot size was 1 × 6 mm^2. The x-ray flux was significantly reduced using Al filters to ensure no x-ray induced damage was observed (as assessed from the comparison of subsequently measured spectra at a fixed sample position). All reported spectra reflect the average of at least two individual scans.

The reference complexes shown in Scheme 1(a) were measured as pellets, prepared from powders diluted in sucrose (2.4% Re by mass, finely ground). Re^{+1}-chloro and Re^{+1}-aqua were prepared and measured in air, while Re^0-anion was kept air-free (prepared and sealed in plastic inside an Ar-filled glove box). All reported XANES

18 July 2023 16:41:10

spectra for the reference complexes were measured in transmission. The reported EXAFS spectra were measured by TFY.

In situ measurements of electrode samples were collected in the one compartment electrochemical cell shown in Figure S1 (SI). In brief, Re@CNT electrodes were used as both working electrodes and x-ray windows. A Kapton film was epoxied on the front side of the electrode to prevent electrolyte leaking. Pt mesh (EF-1355, Bioanalytical Systems) was used as counter and Ag wire as reference electrodes. Electrolyte was 0.5M $KHCO_3$ in deionized water and the electrolyte solution was flowed through the cell using an HPLC pump. All measurements were carried out under inert atmosphere by purging the electrolyte reservoir with Ar. Experiments were performed either under open circuit potential (OCP) or under controlled potential electrolysis at −1.2 V vs Ag/AgCl. All reported XANES and EXAFS spectra for electrode samples were measured by TFY.

All XAS data processing was performed using the Athena software package. All plotted XANES data have a linear background subtracted (from linear fit in 10.39–10.51 keV region). All XANES data were normalized such that the "edge jump" (selected to be 10.539 keV) is 1.0 based on a polynomial fit to the post-edge region (defined from 10.699 to 11.319 keV for all *in situ* data or from 10.569 to 10.639 keV for select reference sample datasets when EXAFS region was not measured). The XANES data were further processed to extract an integrated intensity for the "white line" peak, which is described in detail in the supplementary material, Sec. II (Figs. S3 and S7). For the EXAFS data processing, the window for Fourier transformation was taken from the first zero-crossing point after 2 $Å^{-1}$ until the first zero-crossing point after 13 $Å^{-1}$, unless otherwise noted. A Hanning windowing model was applied. The calculated EXAFS corresponding to single scattering paths [Fig. 2(c)] was determined using the FEFF program[38] within the Artemis program package.[39] The structures used for the EXAFS calculations came from the crystal structure of Re^{+1}-chloro.[15] Re^{+1}-aqua was predicted from the DFT optimized structure of $[Re^{+1}(bpy)(CO)_3(H_2O)]^+$ (LANL2DZ basis set for Re and 6–31 G for main group elements with B3LYP functional). The scattering paths for the closely interacting Re^0-anion and CNT fragment were predicted from their optimized structure shown in Fig. S8 (calculation details below).

Calculations of the closely interacting Re^0-anion/CNT species

The interacting Re^0-anion/CNT species was optimized using density functional theory calculations, carried out using Jaguar v11.2 by Schrödinger, Inc.[40] Calculations were performed using the PBE-D3 functional[41] with the 6-31G*+ basis set and Los Alamos large-core potential (LAV3P*+ in Jaguar).

The calculation included implicit solvent treatment as described by the Poisson–Boltzmann finite element method (PBF) solvation model.[42,43] Solvent parameters matching those of water were used (probe radius = 1.4 Å, dielectric constant = 80.37).

Vibrational frequencies were performed to confirm that the optimized geometry was at a local minimum (0 imaginary frequencies). Figure S8 shows the optimized structure for Re-anion on CNT.

AUTHOR DECLARATIONS

Conflict of Interest

The authors have no conflicts to disclose.

Author Contributions

Marija R. Zoric: Conceptualization (equal); Data curation (lead); Formal analysis (equal); Investigation (lead); Writing – original draft (lead). **Thomas Chan**: Data curation (supporting); Investigation (supporting); Writing – review & editing (supporting). **Charles B. Musgrave III**: Data curation (supporting); Investigation (supporting); Writing – review & editing (supporting). **William A. Goddard III**: Funding acquisition (equal); Supervision (supporting); Writing – review & editing (supporting). **Clifford P. Kubiak**: Conceptualization (supporting); Funding acquisition (equal); Supervision (supporting); Writing – review & editing (supporting). **Amy A. Cordones**: Conceptualization (lead); Data curation (equal); Formal analysis (equal); Funding acquisition (equal); Investigation (equal); Supervision (lead); Writing – original draft (supporting); Writing – review & editing (lead).

DATA AVAILABILITY

The data that support the findings of this study are available from the corresponding author upon reasonable request.

REFERENCES

[1] C. Costentin and J.-M. Savéant, Curr. Opin. Electrochem. **15**, 58 (2019).

[2] D.-H. Nam, P. De Luna, A. Rosas-Hernández, A. Thevenon, F. Li, T. Agapie, J. C. Peters, O. Shekhah, M. Eddaoudi, and E. H. Sargent, Nat. Mater. **19**, 266 (2020).

[3] X.-M. Hu, S. U. Pedersen, and K. Daasbjerg, Curr. Opin. Electrochem. **15**, 148 (2019).

[4] J. Wang, Y. Wang, H. Hu, Q. Yang, and J. Cai, Nanoscale **12**, 4238 (2020).

[5] E. W. Lees, B. A. Mowbray, F. G. Parlane, and C. P. Berlinguette, Nat. Rev. Mater. **7**, 55 (2022).

18 July 2023 16:41:10

[6] Y. Wu, Z. Jiang, X. Lu, Y. Liang, and H. Wang, Nature **575**, 639 (2019).

[7] X. Zhang, Y. Wang, M. Gu, M. Wang, Z. Zhang, W. Pan, Z. Jiang, H. Zheng, M. Lucero, H. Wang, G. E. Sterbinsky, Q. Ma, Y.-G. Wang, Z. Feng, J. Li, H. Dai, and Y. Liang, Nat. Energy **5**, 684 (2020).

[8] F. Xu, L. Zhang, X. Ding, M. Cong, Y. Jin, L. Chen, and Y. Gao, Chem. Commun. **55**, 14111 (2019).

[9] R. N. Schaugaard, K. Raghavachari, and L.-s. Li, Inorg. Chem. **57**, 10548 (2018).

[10] M. N. Jackson and Y. Surendranath, Acc. Chem. Res. **52**, 3432 (2019).

[11] M. N. Jackson, S. Oh, C. J. Kaminsky, S. B. Chu, G. Zhang, J. T. Miller, and Y. Surendranath, J. Am. Chem. Soc. **140**, 1004 (2018).

[12] M. N. Jackson, C. J. Kaminsky, S. Oh, J. F. Melville, and Y. Surendranath, J. Am. Chem. Soc. **141**, 14160 (2019).

[13] S. Oh, J. R. Gallagher, J. T. Miller, and Y. Surendranath, J. Am. Chem. Soc. **138**, 1820 (2016).

[14] M. R. Zoric, E. J. Askins, X. Qiao, and K. D. Glusac, ACS Appl. Electron. Mater. **3**, 854 (2021).

[15] J. M. Smieja, E. E. Benson, B. Kumar, K. A. Grice, C. S. Seu, A. J. M. Miller, J. M. Mayer, and C. P. Kubiak, Proc. Natl. Acad. Sci. U. S. A. **109**, 15646 (2012).

[16] J. M. Smieja and C. P. Kubiak, Inorg. Chem. **49**, 9283 (2010).

[17] J. D. Blakemore, A. Gupta, J. J. Warren, B. S. Brunschwig, and H. B. Gray, J. Am. Chem. Soc. **135**, 18288 (2013).

[18] S. Sinha, A. Sonea, W. Shen, S. S. Hanson, and J. J. Warren, J. Inorg. Chem. **58**, 10454 (2019).

[19] A. Zhanaidarova, A. L. Ostericher, C. J. Miller, S. C. Jones, and C. P. Kubiak, Organometallics **38**, 1204 (2018).

[20] M. L. Clark, P. L. Cheung, M. Lessio, E. A. Carter, and C. P. Kubiak, ACS Catal. **8**, 2021 (2018).

[21] T. R. O'Toole, B. P. Sullivan, M. R.-M. Bruce, L. D. Margerum, R. W. Murray, and T. Meyer, J. Electroanal. Chem. Interfacial Electrochem. **259**, 217 (1989).

[22] A. Zhanaidarova, S. C. Jones, E. Despagnet-Ayoub, B. R. Pimentel, and C. P. Kubiak, J. Am. Chem. Soc. **141**, 17270 (2019).

[23] A. El Nahhas, R. M. Van der Veen, T. J. Penfold, V. T. Pham, F. A. Lima, R. Abela, A. M. Blanco-Rodriguez, S. Zális̆á, A. Vlcáek, I. Tavernelli, U. Rothlisberger, C. J. Milne, and M. Chergui, J. Phys. Chem. A **117**, 361 (2013).

[24] S. Záliš̆, C. J. Milne, A. El Nahhas, A. M. Blanco-Rodríguez, R. M. Vam der Veen, and A. Vlček, Inorg. Chem. **52**, 5775 (2013).

[25] E. E. Benson, M. D. Sampson, K. A. Grice, J. M. Smieja, J. D. Froehlich, D. Friebel, J. A. Keith, E. A. Carter, A. Nilsson, and C. P. Kubiak, Angew. Chem., Int. Ed. **52**, 4841 (2013).

[26] P. Christensen, A. Hamnett, A. V. G. Muir, and J. A. Timney, J. Chem. Soc., Dalton Trans. **1992**, 1455.

[27] J. K. Nganga, L. M. Wolf, K. Mullick, E. Reinheimer, C. Saucedo, M. E. Wilson, K. A. Grice, M. Z. Ertem, and A. M. Angeles-Boza, Inorg. Chem. **60**, 3572 (2021).

[28] H. Wang, P. Ge, C. G. Riordan, S. Brooker, C. G. Woomer, T. Collins, C. A. Melendres, O. Graudejus, N. Bartlett, and S. P. Cramer, J. Phys. Chem. B **102**, 8343 (1998).

[29] K.-i. Shimizu, T. Oda, Y. Sakamoto, Y. Kamiya, H. Yoshida, and A. Satsuma, Appl. Catal., B **111-112**, 509 (2012).

[30] F. W. Lytle, P. S. P. Wei, R. B. Greegor, G. H. Via, and J. H. Sinfelt, J. Chem. Phys. **70**, 4849 (1979).

[31] J. Choi, P. Wagner, S. Gambhir, R. Jalili, D. R. MacFarlane, G. G. Wallace, and D. L. Officer, ACS Energy Lett. **4**, 666 (2019).

[32] M. Zhu, R. Ye, K. Jin, N. Lazouski, and K. Manthiram, ACS Energy Lett. **3**, 1381 (2018).

[33] S. Zhang, T. L. Brown, Y. Du, and J. R. Shapley, J. Am. Chem. Soc. **115**, 6705 (1993).

[34] D. M. Thompson, M. Bengough, and M. C. Baird, Organometallics **21**, 4762 (2002).

[35] C. J. Kaminsky, S. Weng, J. Wright, and Y. Surendranath, Nat. Catal. **5**, 430 (2022).

[36] Y. Wu, G. Hu, C. L. Rooney, G. W. Brudvig, and H. Wang, ChemSusChem **13**, 3283 (2020).

[37] J. Karges, M. Kalaj, M. Gembicky, and S. M. Cohen, Angew. Chem., Int. Ed. **60**, 10716 (2021).

[38] J. J. Rehr and R. C. Albers, Rev. Mod. Phys. **72**, 621 (2000).

[39] B. Ravel and M. Newville, J. Synchrotron Radiat. **12**, 537 (2005).

[40] A. D. Bochevarov, E. Harder, T. F. Hughes, J. R. Greenwood, D. A. Braden, D. M. Philipp, D. Rinaldo, M. D. Halls, J. Zhang, and R. A. Friesner, Int. J. Quantum Chem. **113**, 2110 (2013).

[41] J. P. Perdew, K. Burke, and M. Ernzerhof, Phys. Rev. Lett. **77**, 3865 (1996).

[42] M. Friedrichs, R. Zhou, S. R. Edinger, and R. A. Friesner, J. Phys. Chem. B **103**, 3057 (1999).

[43] D. J. Tannor, B. Marten, R. Murphy, R. A. Friesner, D. Sitkoff, A. Nicholls, B. Honig, M. Ringnalda, and W. A. Goddard, J. Am. Chem. Soc. **116**, 11875 (1994).

18 July 2023 16:41:10